Dear Author,

Please, note that changes made to the HTML content will be added to the article before publication, but are not reflected in this PDF.

Note also that this file should not be used for submitting corrections.

AUTHOR QUERY FORM

ELSEVIER	Journal: HMT Article Number: 11227	Please e-mail or fax your responses and any corrections to: E-mail: corrections.eseo@elsevier.sps.co.in Fax: +31 2048 52799

Dear Author,

Please check your proof carefully and mark all corrections at the appropriate place in the proof (e.g., by using on-screen annotation in the PDF file) or compile them in a separate list. Note: if you opt to annotate the file with software other than Adobe Reader then please also highlight the appropriate place in the PDF file. To ensure fast publication of your paper please return your corrections within 48 hours.

For correction or revision of any artwork, please consult http://www.elsevier.com/artworkinstructions.

Any queries or remarks that have arisen during the processing of your manuscript are listed below and highlighted by flags in the proof. Click on the 'Q' link to go to the location in the proof.

Location in article	Query / Remark: click on the Q link to go Please insert your reply or correction at the corresponding line in the proof
Q1	Please confirm that given name(s) and surname(s) have been identified correctly.
Q2	Please check the edits made in affiliation "b", and correct if necessary.
Q3	Please check whether the designated corresponding author is correct, and amend if necessary.
	Please check this box if you have no corrections to make to the PDF file ☐

Thank you for your assistance.

International Journal of Heat and Mass Transfer xxx (2014) xxx–xxx

Contents lists available at ScienceDirect

International Journal of Heat and Mass Transfer

journal homepage: www.elsevier.com/locate/ijhmt

MHD natural-convection flow in an inclined square enclosure filled with a micropolar-nanofluid

Q1 G.C. Bourantas [a], V.C. Loukopoulos [b,*]

[a] MOSAIC Group, Max Planck Institute of Molecular Cell Biology and Genetics, Dresden, Germany
Q2 [b] Department of Physics, University of Patras, Patras, 26500 Rion, Greece

ARTICLE INFO

Article history:
Received 17 March 2014
Received in revised form 8 August 2014
Accepted 27 August 2014
Available online xxxx

Keywords:
Micropolar
Nanofluids
Magnetohydrodynamics
Natural convection
Meshfree point collocation method

ABSTRACT

Transient, laminar, natural-convection flow of a micropolar-nanofluid (Al_2O_3/water) in the presence of a magnetic field in an inclined rectangular enclosure is considered. A meshless point collocation method utilizing a velocity-correction scheme has been developed. The governing equations in their velocity–vorticity formulation are solved numerically for various Rayleigh (*Ra*) and Hartman (*Ha*) numbers, different nanoparticles volume fractions (φ) of and considering different inclination angles and magnetic field directions. The results show that, both, the strength and orientation of the magnetic field significantly affect the flow and temperature fields. For the cases considering herein, experimentally given forms of dynamic viscosity, thermal conductivity and electrical conductivity are utilized.

1. Introduction

Magnetohydrodynamic (MHD) flows, associated with heat transfer, have received considerable attention over the last decades since there is a growing interest of understanding the underlying physical processes occurring, that is natural convection under the influence of a magnetic field. This is due to their wide variety of application in engineering areas, such as crystal growth in liquid, cooling of nuclear reactor, electronic package, microelectronic devices, and solar technology. There has been an increasing interest to understand the flow behavior and the heat transfer mechanism of enclosures that are filled with electrically conducting fluids under the influence of a magnetic field [1–3]. For an electrically conducting fluid when the magnetic field is present, there are two body forces, a buoyancy force and a Lorentz force. These two forces interact with each other and influence the flow and heat transfer.

Numerical studies have been performed in order to evaluate the effect of the magnetic field on natural convection flow and heat transfer in cavities. Authors in [4] studied the steady state, laminar natural convection flow in the presence of a magnetic field, considering as a study case an inclined rectangular enclosure heated and cooled on adjacent walls. They stated that the magnetic field suppressed the convective flow and the heat transfer rate, while the orientation and the aspect ratio of the enclosure along with both the strength and direction of the magnetic field significantly affected the flow and temperature fields. Authors in [5] numerically studied natural convection occurring in a water filled square cavity under the influence of a magnetic field. They considered temperature dependent physical properties and they observed that both flow and temperature fields were affected by changing the reference temperature parameter when both thermal conductivity and viscosity were temperature dependent. Additionally, they stated that the heat transfer rate was influenced by the direction of the external magnetic field and decreased by an increase of the magnetic field. Authors in [6] conducted a numerical study concerning a magneto-convection flow in a cavity with partially active vertical walls. They found that the average Nusselt number decreases with an increase of Hartmann number (*Ha*), while it increases with the Rayleigh number (*Ra*). Authors in [7] considered the effect of the magnetic field on convection heat transfer inside a tilted square enclosure. Their study showed that the heat transfer mechanism and flow characteristics inside the enclosure depend strongly upon both magnetic field and inclination angle.

In applications where a significant amount of heat needs to be removed from a very small surface, the coolant should have more effective heat transfer characteristics. Due to technological achievements nanomaterials with size ranging from 1 to 100 nm, have been mainly used in the areas of heat transfer, electricity,

Q3 * Corresponding author.
E-mail addresses: bouranta@mpi-cbg.de (G.C. Bourantas), vxloukop@physics.upatras.gr (V.C. Loukopoulos).

http://dx.doi.org/10.1016/j.ijheatmasstransfer.2014.08.075
0017-9310/© 2014 Published by Elsevier Ltd.

HMT 11227
8 September 2014
ARTICLE IN PRESS
No. of Pages 16, Model 5G

Nomenclature

C_p	specific heat at constant pressure (J kg^{-1} K^{-1})
g	gravitational acceleration (m s^{-2})
Ra	Rayleigh number
L	length of the enclosure (m)
k	thermal conductivity (W m^{-1} K^{-1})
Nu	Nusselt number
p	pressure
Pr	Prandtl number
T	dimensional temperature (°C)
u,v	dimensional velocity (m s^{-1})
U,V	dimensionless velocity components
x,y	dimensional coordinates (m)
X,Y	dimensionless coordinates

Greek symbols

α	thermal diffusivity (m^2 s^{-1})
β	thermal expansion coefficient (K^{-1})
θ	dimensionless temperature
μ	dimensionless thermal conductivity
$\rho \varphi$	density (kg m^{-3})relative nanoparticle volumetric fraction
ω	dimensional vorticity (s^{-1})
Ω	dimensionless vorticity
γ	angle of inclination of the enclosure from the horizontal axis
ξ	angle of orientation of the magnetic
τ	dimensionless time

Subscripts

avg	average
C	cold
H	hot
F	base fluid
P	particle
nf	nanofluid

magnetism and mechanics. These nanoscale particles, such as oxide ceramics, nitride ceramics, carbide ceramics, metals and semiconductors, when suspended in a base fluid such as water, ethylene, glycol, engine oil or refrigerant form the so-called nanofluids [8]. In the numerical studies for natural convective heat transfer of nanofluids conducted by several researchers, nanofluids were treated as a single-phase fluid and conventional equations of mass, momentum and energy were solved. Authors in [9] studied natural convection of Cu-water nanofluid in a two-dimensional enclosure assuming uniform volume fraction. The mass and momentum equations were solved in their stream function-vorticity formulation and it was stated that Nusselt number increases with an increase of the volume fraction of the nanoparticles. In [10] a study of natural convection in horizontal annuli using different nanofluids took place and showed that the heat transfer is enhanced by using nanofluids. In fact the Nusselt number increases with increasing nanoparticles volume fraction. In Oztop and Abu-Nada [11] authors studied the natural convection of a nanofluid being in a partially heated enclosures considering different aspect ratios. They found that the heat transfer was more pronounced at low aspect ratio and high volume fraction of nanoparticles. Aminossadati and Ghasemi [12] considered the effect of apex angle, position and dimension of heat source on fluid flow and heat transfer in a triangular enclosure using nanofluid. They found that at low Rayleigh numbers, the heat transfer rate continuously increases with the enclosure apex angle and decreases with the distance of the heat source from the left vertex.

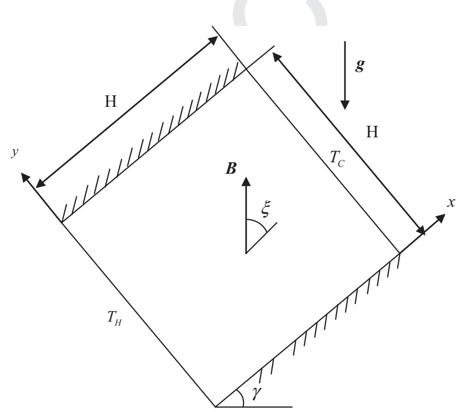

Fig. 1. Geometry and coordinate system.

Most of the studies which focus on the natural convection in enclosures with magnetic effects have considered an electrically conducting fluid with low thermal conductivity. This limits the enhancement of heat transfer in the enclosure especially when a magnetic field is applied. There are several studies dealing with the nanofluids heat transfer that state totally different findings. Most researchers argue that the addition of nanoparticles with relatively higher thermal conductivity to the base fluid results in an increase of the thermal performance of the resultant nanofluid [13–15]. On the other hand, some researchers argue that the dispersion of nanoparticles in the base fluid may result in a decrease of the heat transfer [16]. The numerical studies and experimental findings in the case of natural convection in enclosures are controversial. Therefore, it is possible that the assumptions made in the theoretical models lead to false outcomes. The enhancement or mitigation of the heat transfer of nanofluids may be because of the formulae used for their thermal properties. A comprehensive nanofluid simulation study should take account of the structure, shape, size, aggregation and anisotropy of the nanoparticles as well as the type, fabrication process, particle aggregation and deterioration of nanofluids. A fluid theory that potential can bridge the gap between the numerical and experimental finding is the micropolar flow theory. Micropolar fluids, introduced by Eringen [17], take into account the microstructure of the fluid along with the inertial characteristics of the substructure particles, which are allowed to undergo rotation. In such way nanofluids can be considered as a fluid medium whose properties and behavior are strongly influenced by the local motions of the material particles contained in each of its volume elements.

In the present paper we incorporate the micropolar flow theory to study the natural convection of an electrically conducted nanofluid in a square cavity subjected to a magnetic field. The work in

Table 1
Thermo-physical properties of water and nanoparticles.

	ρ(kgr/m^3)	C_p(J/kgrK)	k(W/mK)	$\beta \times 10^{-5}$(K^{-1})
Pure Water	997.1	4179	0.613	21
Alumina (Al_2O_3)	3970	765	40	0.85

Please cite this article in press as: G.C. Bourantas, V.C. Loukopoulos, MHD natural-convection flow in an inclined square enclosure filled with a micropolar-nanofluid, Int. J. Heat Mass Transfer (2014), http://dx.doi.org/10.1016/j.ijheatmasstransfer.2014.08.075

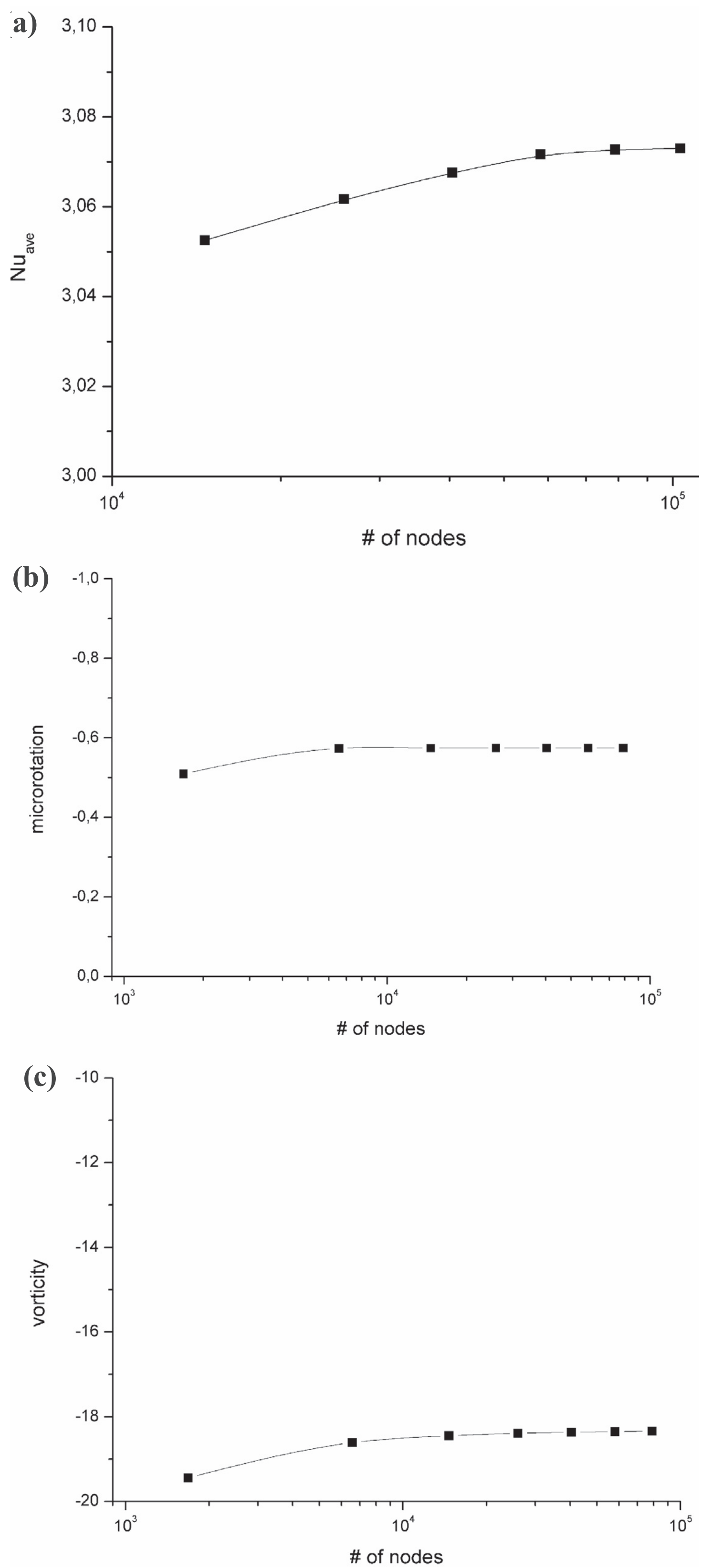

Fig. 2. Convergence analysis for the case of $K = 2$, $Ha = 60$, $Ra = 10^4$and $\varphi = 0.03$ for **(a)** average Nusselt number **(b)** microrotation and **(c)** vorticity.

[18] has been extended, considering that nanofluid has an electrical conductivity and incorporating suitably the influence of the applied magnetic field in equations of the flow. An Al_2O_3/water nanofluid has been used due to available experimentally derived relations for the thermo-physical properties of the nanofluid, that is, thermal conductivity, dynamic viscosity and electrical

Table 2a
Numerical results for the local Nusselt number for various inclination angles using Finite Volume Method (FVM).

φ	Gr	Nu (Ha = 0)	Nu (Ha = 100)		
			φ = 0°	φ = 45°	φ = 90°
0°	10^3	3.745834	3.681442	3.676955	3.678740
	10^4	4.771623	3.683067	3.681906	3.681277
	10^5	6.677280	3.824211	3.944665	3.885215
	10^6	N/A	6.766862	N/A	N/A
−45°	10^3	3.755500	3.682916	3.680122	3.680210
	10^4	4.552761	3.680572	3.684567	3.684299
	10^5	6.379730	3.854637	3.877413	3.875004
	10^6	9.997426	N/A	6.151953	N/A
45°	10^3	3.682832	3.680268	3.681467	3.680166
	10^4	4.334201	3.678017	3.682005	3.680053
	10^5	5.686973	3.703160	3.683273	3.711887
	10^6	N/A	N/A	N/A	N/A

Table 2b
Numerical results for the local Nusselt number for various inclination angles using the Meshless Point Collocation (MPC) method.

φ	Gr	Nu (Ha = 0)	Nu (Ha = 100)		
			φ = 0°	φ = 45°	φ = 90°
0°	10^3	3.73583	3.669983	3.681255	3.668332
	10^4	4.76083	3.678857	3.679896	3.680025
	10^5	6.68012	3.830211	3.939895	3.879315
	10^6		6.758962		
−45°	10^3	3.742293	3.675116	3.678522	3.675810
	10^4	4.514968	3.690238	3.688685	3.690359
	10^5	6.290098	3.860638	3.887543	3.882854
	10^6	9.986437		6.149953	
45°	10^3	3.673349	3.680532	3.680025	3.670576
	10^4	4.329640	3.669087	3.673368	3.682053
	10^5	5.680058	3.710160	3.680465	3.709757

conductivity. In Section 2, the governing equations of the proposed micropolar nanofluid model are presented. Section 3 describes the Moving Least Squares (MLS) approximation methods and the algorithm used, while details of the numerical technique are presented in the Appendix. In Section 4 the validation of the proposed scheme is depicted. In Section 5, the heat transfer performance of a micropolar nanofluid enclosed in a rectangular cavity is studied for a range of solid volume fractions $(0 \leqslant \varphi \leqslant 0.05)$, Hartmann numbers $(0 \leqslant Ha \leqslant 120)$, Rayleigh numbers $(10^3 \leqslant Ra \leqslant 10^6)$ and, orientation $(0 \leqslant \xi \leqslant 60^o)$ along with inclination angles $(0 \leqslant \gamma \leqslant 60^o)$. For all simulations, pure water is considered as the base fluid with $Pr = 6.2$. Finally, in Section 6, the conclusions complete the paper.

Table 3
Average Nusselt number at various Hartmann (Ha) numbers and volume fraction (φ) with $Ra = 10^5$. First line for the results of FVM and second line for MPCVC method.

		φ = 0	φ = 0.02	φ = 0.04	φ = 0.06
Ha = 0	Nu_m	4.738	4.820	4.896	4.968
		4.739	4.818	4.894	4.965
	$\lvert\Psi\rvert_{max}$	11.053	11.313	11.561	11.801
		11.018	10.920	11.559	11.798
Ha = 15	Nu_m	4.143	4.179	4.211	4.239
		4.142	4.170	4.211	4.238
	$\lvert\Psi\rvert_{max}$	8.484	8.615	8.734	8.842
		8.480	8.608	8.725	8.824
Ha = 30	Nu_m	3.150	3.138	3.124	3.108
		3.148	3.128	3.122	3.109
	$\lvert\Psi\rvert_{max}$	5.710	5.682	5.642	5.591
		5.711	5.682	5.634	5.584
Ha = 45	Nu_m	2.369	2.342	2.317	2.293
		2.345	2.335	2.315	2.284
	$\lvert\Psi\rvert_{max}$	3.825	3.729	3.629	3.525
		3.815	3.658	3.512	3.485
Ha = 60	Nu_m	1.851	1.831	1.815	1.806
		1.827	1.849	1.872	1.895
	$\lvert\Psi\rvert_{max}$	2.623	2.518	2.415	2.314
		2.615	2.483	2.360	2.246

Please cite this article in press as: G.C. Bourantas, V.C. Loukopoulos, MHD natural-convection flow in an inclined square enclosure filled with a micropolar-nanofluid, Int. J. Heat Mass Transfer (2014), http://dx.doi.org/10.1016/j.ijheatmasstransfer.2014.08.075

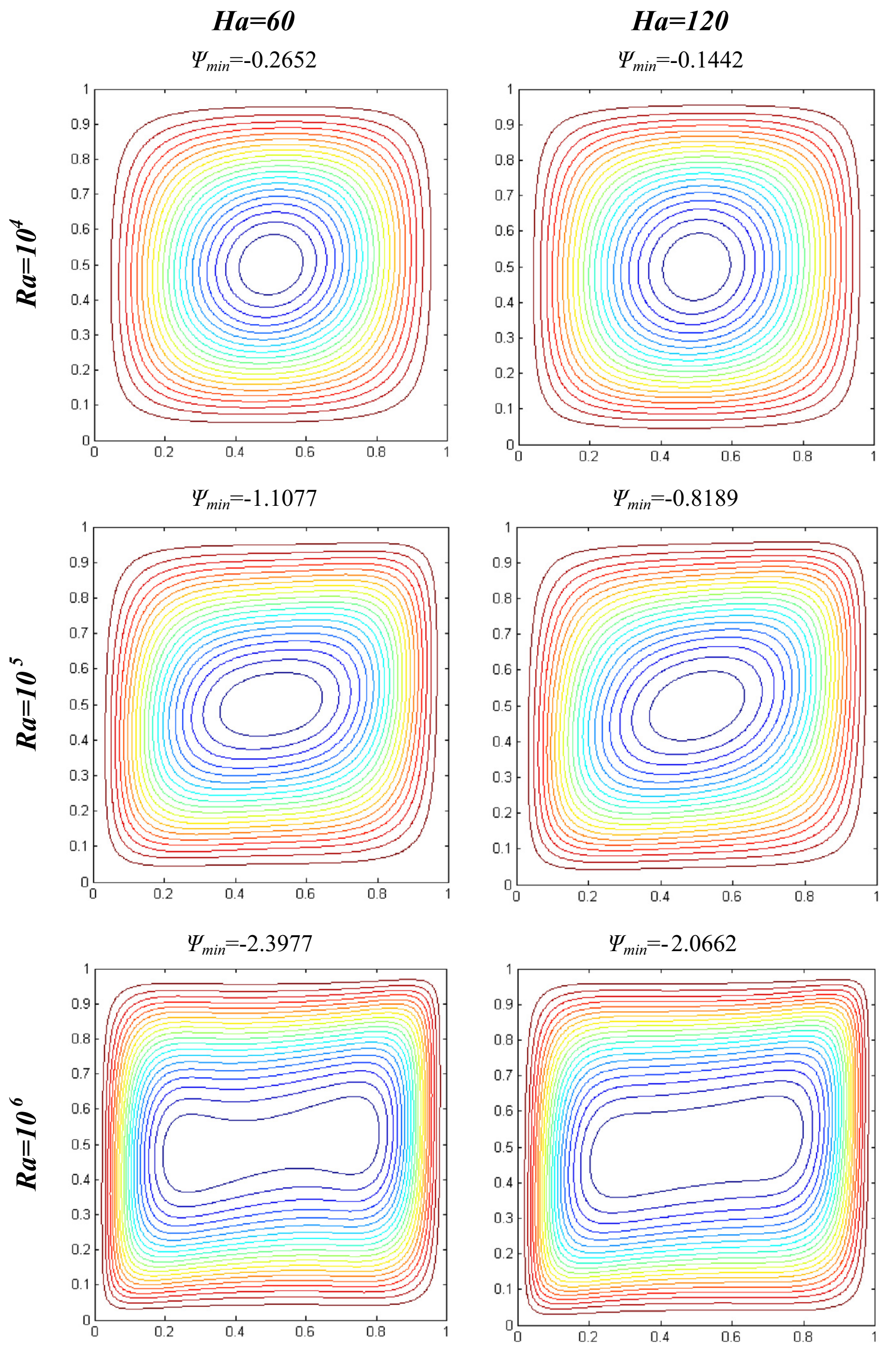

Fig. 3. Streamlines contours for Hartmann numbers $Ha = 60$ and $Ha = 120$, with Rayleigh number given as $Ra = 10^4$, $Ra = 10^5$ and $Ra = 10^6$.

2. Problem formulation

We consider transient, laminar, incompressible natural convection flow in the presence of a magnetic field in an inclined square enclosure of length H filled with micropolar-nanofluid of Al_2O_3/water. The geometry and the coordinate system are schematically shown in Fig. 1. The angle of inclination of the enclosure from the horizontal axis is denoted by γ. A magnetic field of strength $\boldsymbol{B}$ is applied at an angle ξ, with respect to the coordinate system. The top and the bottom walls are insulated and the fluid is isothermally heated and cooled by the left side and right side walls at uniform temperatures of T_H and T_C, respectively.

The physical properties of the fluid are assumed to be constant except the density in the buoyancy force term, which is estimated by the Boussinesq's model. For the latter we can write for the buoyancy term $(\rho - \rho_0)\mathbf{g} \approx -\rho_0\beta(T - T_0)\mathbf{g}$, where ρ_0 is the constant density of the flow, T_0 is the operating temperature and, β is the thermal expansion coefficient. The thermophysical properties of the nanofluid are listed in Table 1. For a micropolar electrically conductive nanofluid under the influence of an external magnetic field for the conservation of mass, linear momentum, angular momentum and in the case of natural convection conservation of energy, the models presented in [18,19] are extended as:

$$\nabla \cdot \mathbf{u} = 0, \tag{1}$$

Please cite this article in press as: G.C. Bourantas, V.C. Loukopoulos, MHD natural-convection flow in an inclined square enclosure filled with a micropolar-nanofluid, Int. J. Heat Mass Transfer (2014), http://dx.doi.org/10.1016/j.ijheatmasstransfer.2014.08.075

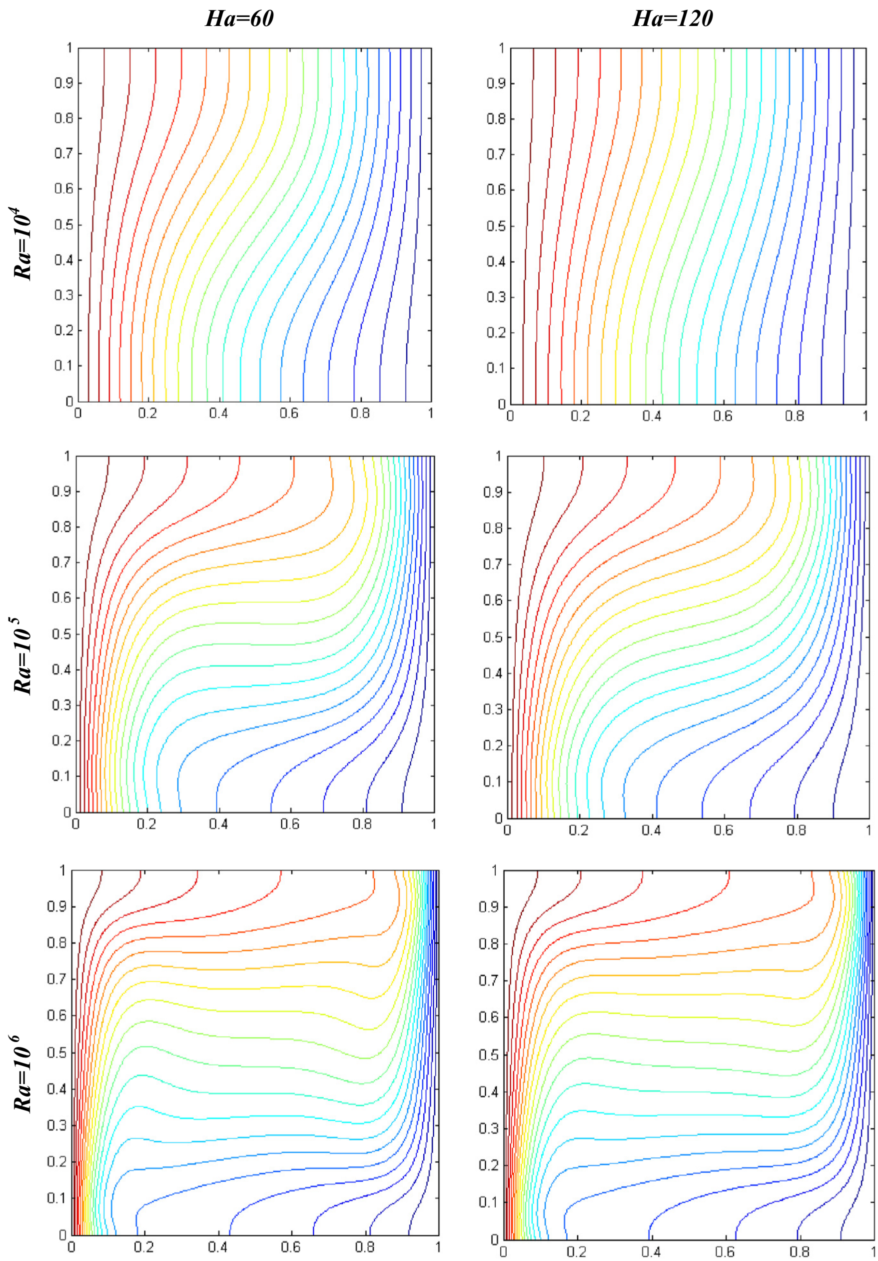

Fig. 4. Temperature contours for Hartmann numbers $Ha = 60$ and $Ha = 120$, with Rayleigh number given as $Ra = 10^4$, $Ra = 10^5$ and $Ra = 10^6$.

$$\rho_{nf}\left(\frac{\partial \boldsymbol{u}}{\partial \boldsymbol{t}} + (\boldsymbol{u}\cdot\boldsymbol{\nabla})\boldsymbol{u}\right) = -\boldsymbol{\nabla} p + (\mu_{nf}+\kappa)\nabla^2\boldsymbol{u} + \kappa\nabla\times\boldsymbol{N} - \boldsymbol{g}((\rho\beta_T)_{nf}(T-T_0)) + \boldsymbol{J}\times\boldsymbol{B}, \quad (2)$$

$$\rho_{nf} j\left(\frac{\partial \boldsymbol{N}}{\partial \boldsymbol{t}} + \boldsymbol{u}\cdot\boldsymbol{\nabla}\right)\boldsymbol{N} = \gamma_{nf}\nabla^2\boldsymbol{N} + \kappa\boldsymbol{\nabla}\times\boldsymbol{u} - 2\kappa\boldsymbol{N}, \quad (3)$$

$$\frac{\partial T}{\partial t} + \boldsymbol{u}\cdot\boldsymbol{\nabla}T = \alpha_{nf}\nabla^2 T, \quad (4)$$

where $\boldsymbol{u} = (u,v)$ is the velocity vector with u and v being the velocity components along x and y axes, p is the pressure, T is the fluid temperature, $\boldsymbol{N}$ is the microrotation vector, $\boldsymbol{g}$ is the acceleration due to gravity, ρ_{nf} is the density, μ_{nf} is the dynamic viscosity, κ is the vortex viscosity, γ_{nf} is the spin-gradient viscosity, j is the micro-inertia density, α_{nf} is the thermal diffusivity of the nanofluid, $\boldsymbol{B}$ is magnetic field and $\boldsymbol{J}$ is the current density which, in the absence of an electric field, can be written as

$$\boldsymbol{J} = \sigma_{nf}(\boldsymbol{u}\times\boldsymbol{B}). \quad (5)$$

In the present simulations, the magnetic Reynolds number was assumed to be small and the induced magnetic field due to the motion of the electrically conducting fluid was neglected [20]. The Joule heating of the fluid and the effect of viscous dissipation were also considered to be negligible.

By applying the curl operator to the vorticity, defined as $\boldsymbol{\omega} = \boldsymbol{\nabla}\times\boldsymbol{u}$ and, using the mass conservation equation ($\boldsymbol{\nabla}\cdot\boldsymbol{u} = 0$) for the incompressible fluid flow we get an elliptic Poisson equation for the velocity

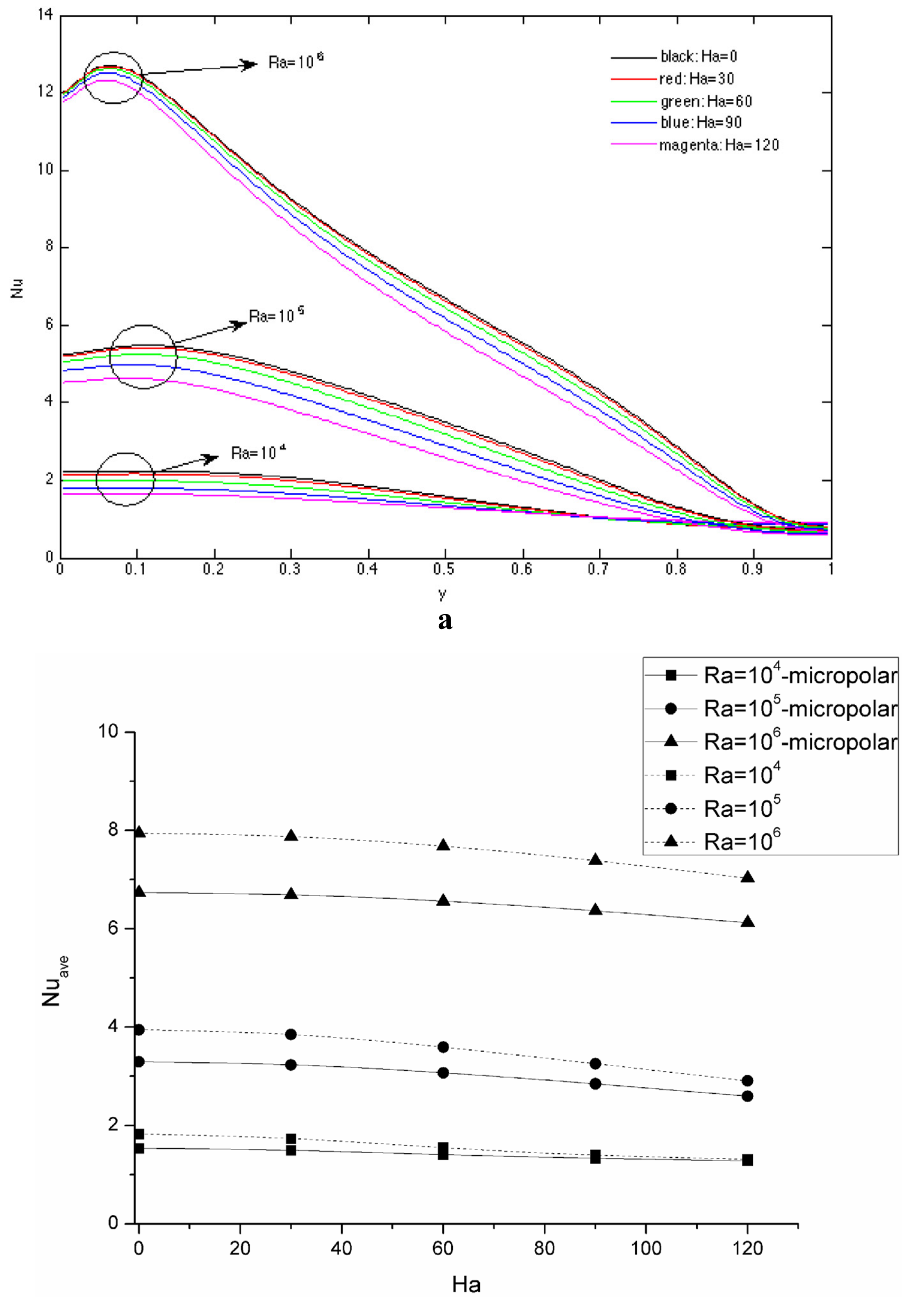

Fig. 5. **(a)** Local Nusselt number along the hot wall for various Rayleigh (Ra) and Hartmann (Ha) numbers and **(b)** average Nusselt number plot versus Hartmann number (Ha) with different Rayleigh (Ra) numbers for a micropolar nanofluid (solid line) and a nanofluid (dashed line).

$$\nabla^2 \boldsymbol{u} + \nabla \times \boldsymbol{\omega} = 0. \tag{6}$$

Additionally, we can apply the curl operator to the momentum conservation equation (Eq. (2)), taking into consideration that $\nabla \cdot \boldsymbol{\omega} = 0$ and $\nabla \cdot \boldsymbol{N} = 0$, due to the vorticity and microrotation definition, along with $\nabla \cdot \boldsymbol{u} = 0$ due to mass conservation equation. Finally, for the case of two-dimensional plane flow and accounting for all previous assumptions the governing equations, in the velocity–vorticity formulation, can be written as:

$$\nabla^2 u = -\frac{\partial \omega}{\partial y}, \tag{7}$$

$$\nabla^2 v = \frac{\partial \omega}{\partial x}, \tag{8}$$

$$\begin{aligned}\rho_{nf}\left(\frac{\partial \omega}{\partial t} + \boldsymbol{u} \cdot \nabla \omega\right) &= (\mu_{nf} + \kappa)\nabla^2 \omega - \kappa \nabla^2 \mathrm{N} \\ &\quad + g(\rho\beta_T)_{nf}\left(\cos(\gamma)\frac{\partial T}{\partial x} - \sin(\gamma)\frac{\partial T}{\partial y}\right) \\ &\quad + \sigma_{nf}B^2\left(\sin(\xi)\cos(\xi)\frac{\partial u}{\partial x} - \cos^2(\xi)\frac{\partial v}{\partial x}\right) \\ &\quad + +\sigma_{nf}B^2\left(\sin^2(\xi)\frac{\partial u}{\partial y} - \sin(\xi)\cos(\xi)\frac{\partial v}{\partial y}\right)\end{aligned} \tag{9}$$

$$\rho_{nf} j\left(\frac{\partial N}{\partial t} + \boldsymbol{u} \cdot \nabla N\right) = \gamma_{nf}\nabla^2 N - 2\kappa N + \kappa \omega, \tag{10}$$

$$\frac{\partial T}{\partial t} + \boldsymbol{u} \cdot \nabla T = \alpha_{nf}\nabla^2 T, \tag{11}$$

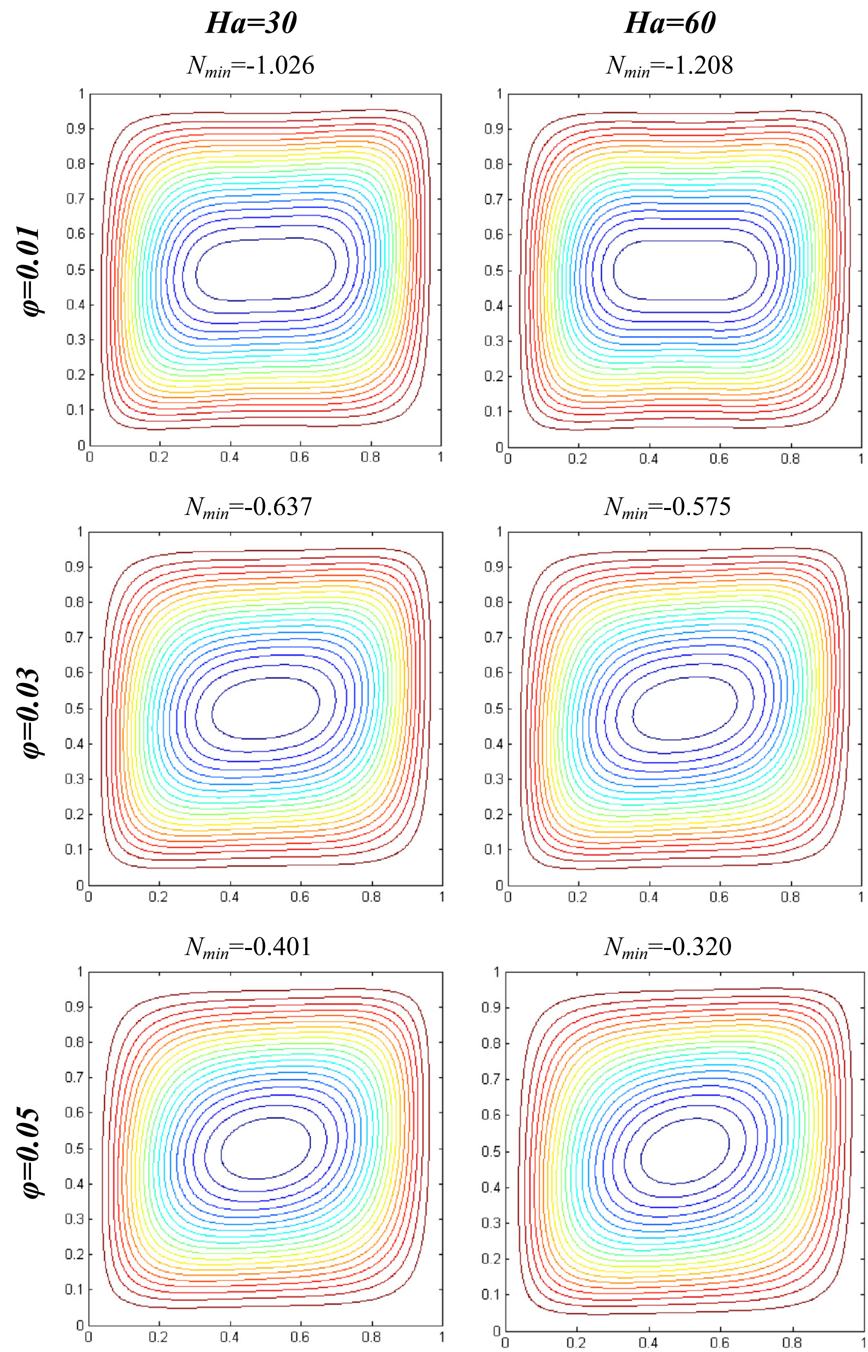

Fig. 6. Microrotation contours (20 isocontours) for Hartmann numbers $Ha = 30$ and $Ha = 60$ having different volume fractions.

Further, we assume that γ_{nf} has the following form as proposed in [21,22]

$$\gamma_{nf} = \left(\mu_{nf} + \frac{\kappa}{2}\right)j. \tag{12}$$

The effective density of the nanofluid is given as

$$\rho_{nf} = (1-\varphi)\rho_f + \varphi\rho_p \tag{13}$$

and the effective dynamic viscosity of the nanofluid given by

$$\mu_{nf} = \mu_f(1 + 39.11\varphi + 533.9\varphi^2), \tag{14}$$

measured experimentally by Pak and Cho [23]. The effective diffusivity of the nanofluid is

$$a_{nf} = \frac{k_{nf}}{(\rho C_p)_{nf}}, \tag{15}$$

where the heat capacitance of the nanofluid is given as

$$(\rho C_p)_{nf} = (1-\varphi)(\rho C_p)_f + \varphi(\rho C_p)_p. \tag{16}$$

The thermal expansion coefficient of the nanofluid can be determined as

$$(\rho\beta)_{nf} = (1-\varphi)(\rho\beta)_f + \varphi(\rho\beta)_p. \tag{17}$$

In Eq. (15), k_{nf} is the thermal conductivity of the nanofluid which has been calculated experimentally [23] and is given by:

$$k_{nf} = k_f(1 + 7.47\varphi). \tag{18}$$

Please cite this article in press as: G.C. Bourantas, V.C. Loukopoulos, MHD natural-convection flow in an inclined square enclosure filled with a micropolar-nanofluid, Int. J. Heat Mass Transfer (2014), http://dx.doi.org/10.1016/j.ijheatmasstransfer.2014.08.075

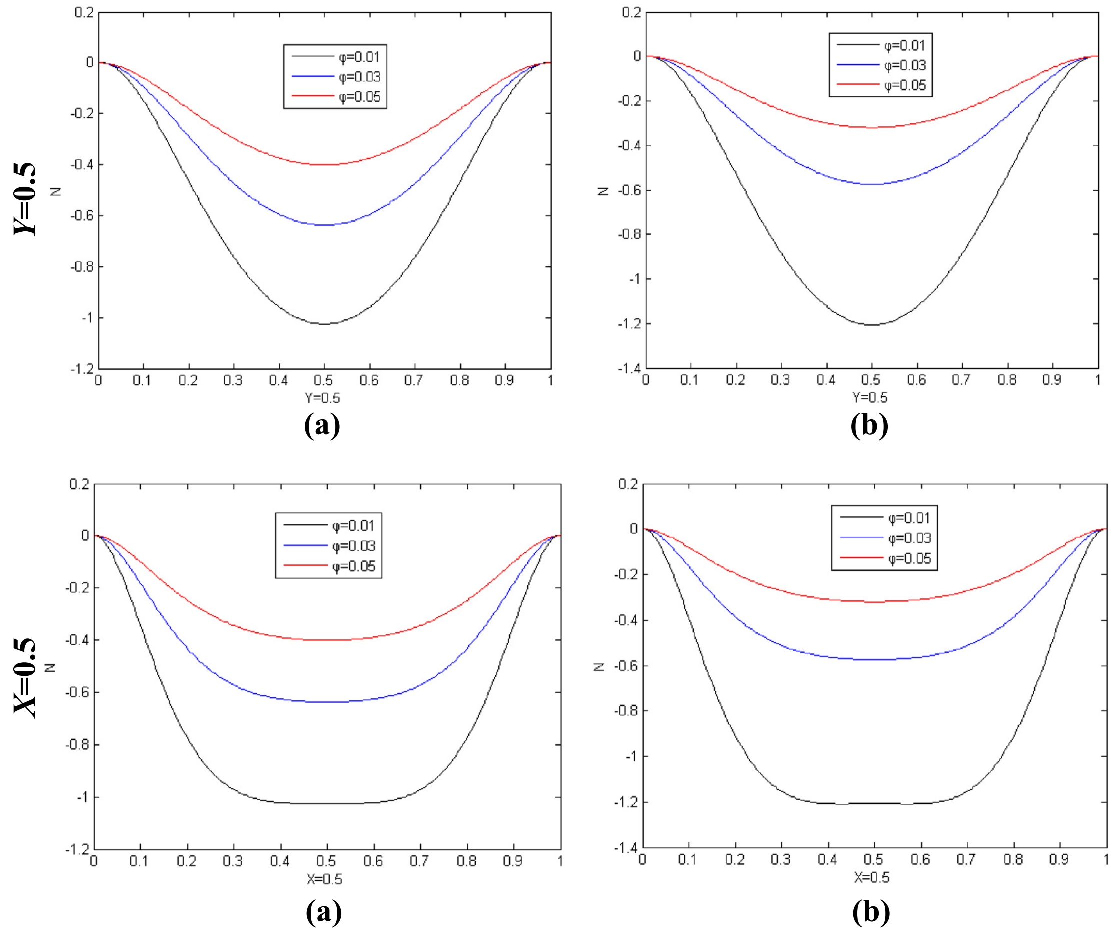

Fig. 7. Microrotation profiles are plotted along the centerlines of the cavity, at $y = 0.5$ and $x = 0.5$, respectively.

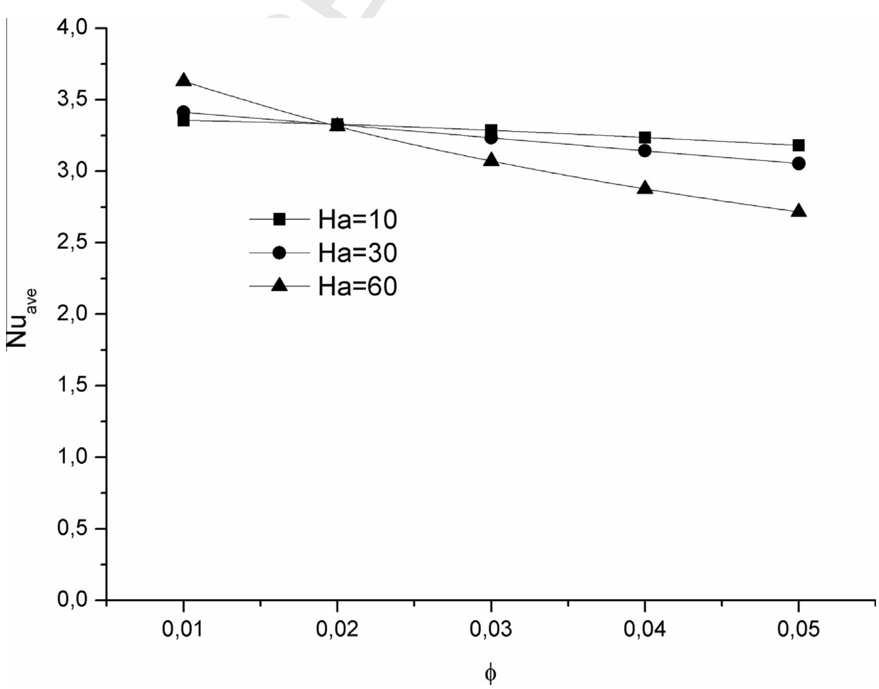

Fig. 8. Average Nusselt number (Nu_{ave}) for different volume fractions.

The base fluid (de-ionized water) electrical conductivity can be considered as negligible. Therefore, it can be safely stated that alumina nanoparticles are the major contributor towards the electrical conductivity of alumina nanofluid, calculated experimentally in [24]

$$\sigma_{nf} = 2982.7\varphi + 57.818 \tag{19}$$

The boundary and initial conditions for the natural convection problem under investigation are set as

$$\begin{aligned}
&t = 0: u = v = 0,\ N = 0,\ T = 0\\
&t > 0: u = v = 0,\ T = T_H,\ N = 0 \quad \text{for } x = 0,\ 0 \le y \le 1\\
&\qquad u = v = 0,\ T = T_C,\ N = 0 \quad \text{for } x = 1,\ 0 \le y \le 1\\
&\qquad u = v = 0,\ \frac{\partial T}{\partial y} = 0,\ N = 0 \quad \text{for } y = 0,1, 0 \le x \le 1
\end{aligned} \tag{20}$$

Introducing the following non-dimensional variables

$$\begin{aligned}
&\tau = \frac{v_f}{H^2}t, (X,Y) = \frac{(x,y)}{H}, \quad (U,V) = \frac{H}{v_f}(u,v),\\
&(N,\Omega) = \frac{H^2}{v_f}(N,\omega), \quad \theta = \frac{T - T_C}{T_H - T_C}, \quad j = H^2
\end{aligned} \tag{21}$$

for the case of two-dimensional flow and, accounting for all previous assumptions the final form of equations is written as follows:

$$\nabla^2 U = -\frac{\partial \Omega}{\partial Y}, \tag{22}$$

$$\nabla^2 V = \frac{\partial \Omega}{\partial X}, \tag{23}$$

$$\begin{aligned}
\frac{\partial \Omega}{\partial \tau} + \boldsymbol{U}\cdot\nabla\Omega = {}& \left(\frac{\mu_{nf}}{\mu_f} + K\right)\left(\frac{\rho_f}{\rho_{nf}}\right)\nabla^2\Omega - K\left(\frac{\rho_f}{\rho_{nf}}\right)\nabla^2 N\\
&+ \frac{Ra}{Pr}\left(\frac{(\rho\beta)_{nf}}{(\rho\beta)_f}\right)\left(\frac{\rho_f}{\rho_{nf}}\right)\left(\cos(\gamma)\frac{\partial\theta}{\partial X} - \sin(\gamma)\frac{\partial\theta}{\partial Y}\right)\\
&+ \left(\frac{\sigma_{nf}}{\sigma_f}\right)\left(\frac{\rho_f}{\rho_{nf}}\right)Ha^2\left(\sin(\xi)\cos(\xi)\frac{\partial U}{\partial X} - \cos^2(\xi)\frac{\partial V}{\partial X}\right)\\
&+ \left(\frac{\sigma_{nf}}{\sigma_f}\right)\left(\frac{\rho_f}{\rho_{nf}}\right)Ha^2\left(\sin^2(\xi)\frac{\partial U}{\partial Y} - \sin(\xi)\cos(\xi)\frac{\partial V}{\partial Y}\right)
\end{aligned} \tag{24}$$

$$\begin{aligned}
\frac{\partial N}{\partial \tau} + \boldsymbol{U}\cdot\nabla N = {}& \left(\frac{\mu_{nf}}{\mu_f} + \frac{K}{2}\right)\left(\frac{\rho_f}{\rho_{nf}}\right)\nabla^2 N - 2K\left(\frac{\rho_f}{\rho_{nf}}\right)N\\
&+ K\left(\frac{\rho_f}{\rho_{nf}}\right)\Omega,
\end{aligned} \tag{25}$$

$$\frac{\partial\theta}{\partial\tau} + \boldsymbol{U}\cdot\nabla\theta = \left(\frac{k_{nf}}{k_f}\right)\left(\frac{(\rho C_p)_f}{(\rho C_p)_{nf}}\right)\frac{1}{Pr}\nabla^2\theta, \tag{26}$$

where $K = \frac{\kappa}{\mu_f}$ is the material parameter, $Pr = \frac{v_f}{a_f}$ is the Prandtl number, $Ra = \frac{g\rho\beta_f\Delta TH^3}{a_f v_f}$ is the Rayleigh number and $Ha = B_0 L\sqrt{\frac{\sigma_f}{\mu_f}}$ is the Hartmann number. The Nusselt number can be expressed as

$$Nu = \frac{h_f H}{k_{nf}}. \tag{27}$$

Regarding to heat transfer between a surface and a fluid flowing past it, a thermal boundary layer develops if the fluid free stream temperature and the surface temperatures differ. In fact, a temperature profile exists due to the energy exchange resulting from this temperature difference.

The convective heat transfer rate per area is expressed as

$$q_w = h_f(T_H - T_C). \tag{28}$$

and because heat transfer at the surface is by conduction

$$q_w = -k_f\frac{\partial}{\partial x}(T - T_C). \tag{29}$$

By substituting Eqs. (28), (29) into Eq. (27), and using the dimensionless quantities, the Nusselt number on the left wall is written as

$$Nu = -\frac{k_{nf}}{k_f}\frac{\partial\theta}{\partial x}. \tag{30}$$

The average Nusselt number is defined as

$$Nu_{ave} = \int_0^1 Nu\,dy. \tag{31}$$

3. Moving Least Squares approximation and solution procedure

3.1. Moving Least Squares

The non-dimensional governing equations were discretized using the meshless point collocation method. The Moving Least Squares (MLS) method [25] was used for the approximation of the unknown field functions, namely velocity components, temperature and microrotation. In the context of the meshless approximation method schemes, the MLS method is widely used, since it can directly approximate the field variables in a local manner and, additionally, can easily be extended to n-dimensional problems.

In the context of the MLS method, an unknown field function $u(\boldsymbol{x})$ is approximated by $u^h(\boldsymbol{x})$ is expressed as

$$u^h(\boldsymbol{x}) = \sum_{i=1}^{m} p_i(\boldsymbol{x})\alpha_i(\boldsymbol{x}) = \boldsymbol{p}^T(\boldsymbol{x})\boldsymbol{a}(\boldsymbol{x}) \tag{32}$$

where $\boldsymbol{p}^{\mathbf{T}}(\boldsymbol{x})$ is a polynomial basis in the space coordinates, and m is the total number of the terms in the basis (herein $m = 6$ since we use a second order polynomial basis) and $\alpha(\boldsymbol{x})$ is the vector of coefficients. The polynomial basis can be written as

$$\begin{aligned}
\boldsymbol{p}^{\boldsymbol{T}}(\boldsymbol{x}) &= \boldsymbol{p}^{\boldsymbol{T}}(\boldsymbol{x} - \boldsymbol{x}_i)\\
&= [1, (x - x_i), (y - y_i), (x - x_i)^2, (x - x_i)(y - y_i), (y - y_i)^2]
\end{aligned} \tag{33}$$

in 2D problems.

There exists a unique local approximation associated with each point in the domain. In order to determine the form of $\alpha(\boldsymbol{x})$, a weighted discrete error norm is constructed and minimized.

Finally, the approximation function takes the form

$$\boldsymbol{u}^h(\boldsymbol{x}) = \sum_{i=1}^{n}\varphi_i(\boldsymbol{x})\,\boldsymbol{u}_i = \boldsymbol{p}^T(\boldsymbol{x})\boldsymbol{A}^{-1}(\boldsymbol{x})\boldsymbol{B}(\boldsymbol{x})\boldsymbol{u} = \boldsymbol{\Phi}^T(\boldsymbol{x})\boldsymbol{u} \tag{34}$$

where the spatial dependence has been lumped into one row matrix, $\boldsymbol{\Phi}^T(\boldsymbol{x})$ and, therefore, the approximation takes the form of a product of a matrix of shape functions with a vector of nodal data, while matrices $\boldsymbol{A}$ and $\boldsymbol{B}$ are defined in [26,27]. Derivatives of the shape functions [26,27] may be calculated by applying the product rule to

$$\boldsymbol{\Phi}^T = \boldsymbol{p}^T\boldsymbol{A}^{-1}\boldsymbol{B}. \tag{35}$$

3.2. Solution procedure and algorithm

For the solution of the Eqs. (22)–(26) the Meshless Point Collocation Velocity-Correction (MPCVC) method presented in [28] is used in relation to the ϑ -weighting method for the spatial and temporal discretization (presented in the Appendix and [29]).

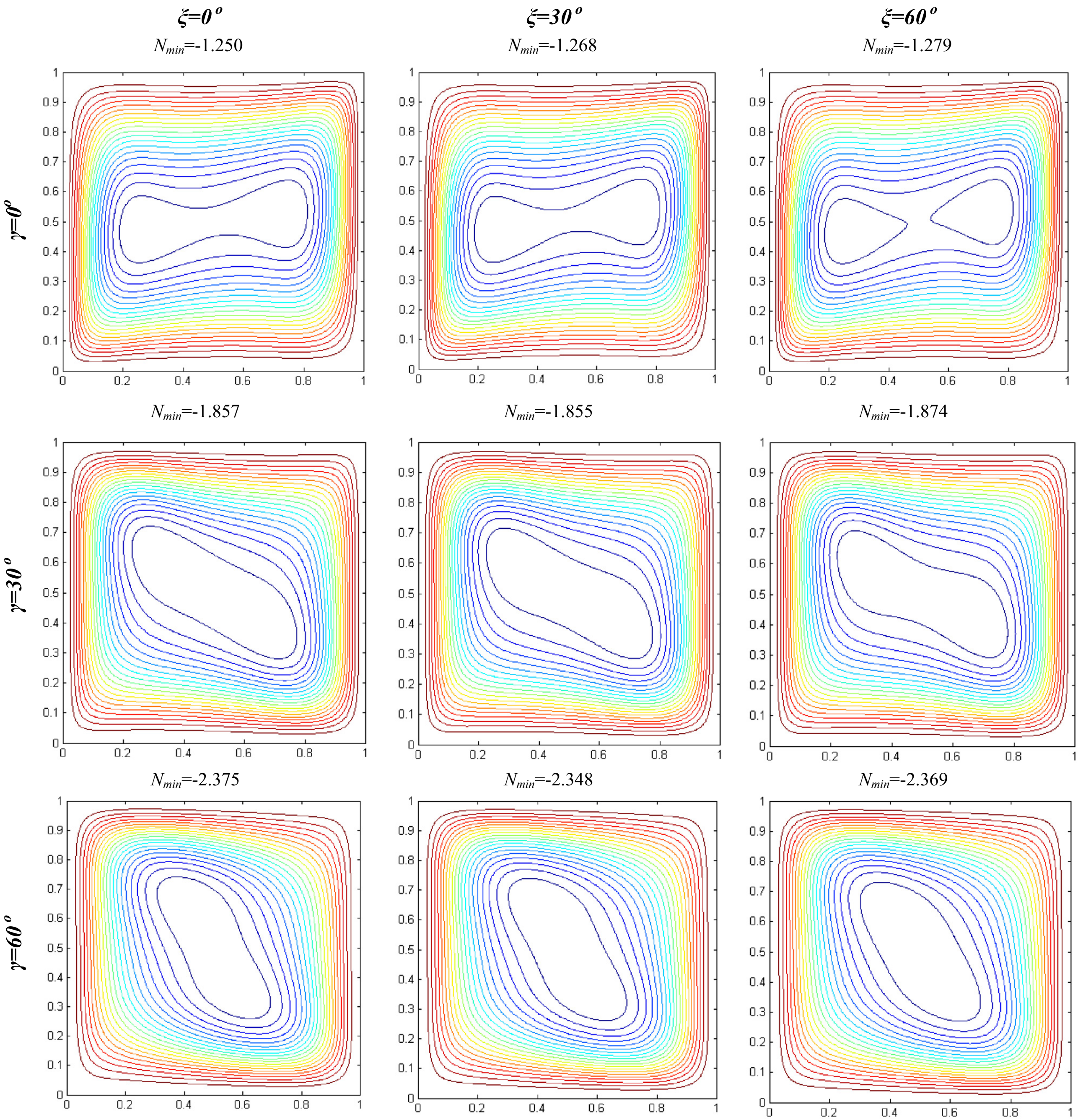

Fig. 9. Microrotation contours for different inclination and magnetic field orientation angles.

After the linearization of the non-linear partial differential Eqs. (21)–(26) and their discretization, the resultant algebraic linear system of equations is solved using an iterative procedure. The steps of the iterative method are described below:

- Set the initial velocity components $u^{(0)}$ and $v^{(0)}$ and calculate the vorticity $\omega^{(0)} = \frac{\partial v^{(0)}}{\partial x} - \frac{\partial u^{(0)}}{\partial y}$.
- Calculate $\frac{\partial \omega^{(0)}}{\partial x}$ and $\frac{\partial \omega^{(0)}}{\partial y}$ and use them to solve the Poisson type equations for the u *and* v velocity component (Eqs. (22) and (23)), using the prescribed boundary conditions. The u^{*} and v^{*} intermediate velocity components are calculated.
- A velocity-correction method [28] is used to calculate the updated velocity components $u^{(k+1)}$ and $v^{(k+1)}$, which satisfy the incompressibility constraint.
- The updated velocity values are used to calculate the temperature field by solving Eq. (26), using the linearization method described above, for the L^{θ} operator (Eq. (A6)). The prescribed temperature boundary conditions are used.
- The updated velocity values are used to calculate the microrotation values by solving Eq. (25), using the linearization method described above, for the L^{N} operator (Eq. (A5)). The prescribed microrotation boundary conditions are used.

Please cite this article in press as: G.C. Bourantas, V.C. Loukopoulos, MHD natural-convection flow in an inclined square enclosure filled with a micropolar-nanofluid, Int. J. Heat Mass Transfer (2014), http://dx.doi.org/10.1016/j.ijheatmasstransfer.2014.08.075

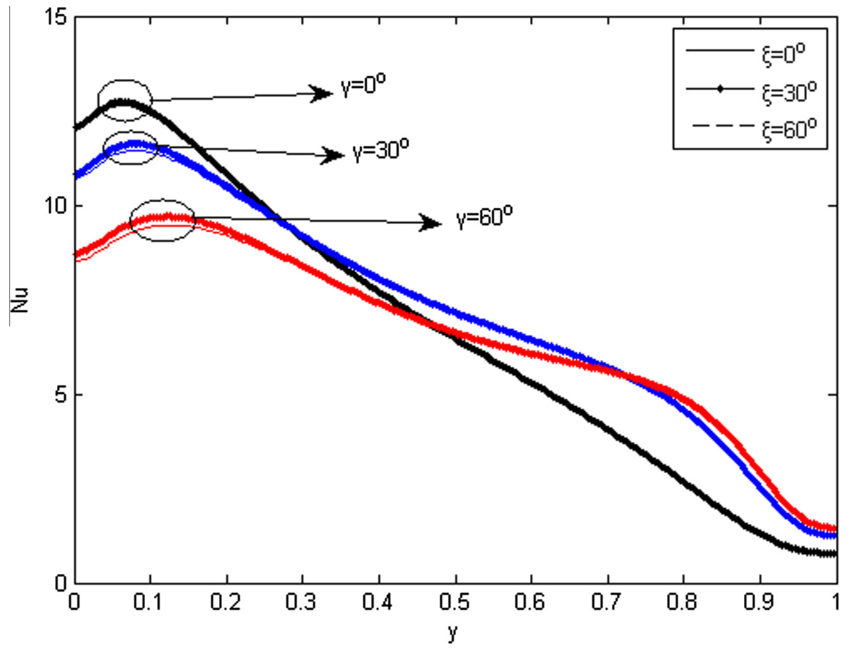

Fig. 10. Local Nusselt number along the hot wall for different magnetic field orientation (ξ) angles for inclination angles **(a)** $\gamma = 0^o$ **(b)** $\gamma = 30^o$ and **(c)** $\gamma = 60^o$.

- The updated velocity and temperature values are used to calculate the vorticity values by solving Eq. (24), using the linearization method described above, for the L^{Ω} operator (Eq. (A6)). The vorticity boundary conditions are calculated by $\omega^{(k+1)} = \frac{\partial v^{(k+1)}}{\partial x} - \frac{\partial u^{(k+1)}}{\partial y}$.
- The L_∞ errors (maximum absolute error) for the u, v, N, θ and Ω are calculated and if their values are less than 10^{-6} the iteration stops.

4. Code validation

A grid independence study took place for the natural convection in the square cavity for $K = 2$, $Ha = 60$, $Ra = 10^5$ and $\varphi = 0.03$ and, as it can be seen in Fig. 2, a grid of size 161×161 (total of 25,921 nodes) satisfies the grid independence. For the sake of accuracy we used a dense grid configuration of 261×261. For the numerical simulations, iterations were stopped when the maximum absolute values (L_∞ norm) of the difference between the successive solutions for velocity components, vorticity, microrotation and temperature at each mesh point are less than 10^{-6}.

In order to validate the present scheme, the steady, laminar natural convection flow in the presence of a magnetic filed in an inclined filled with air is considered [4]. The enclosure is heated (high temperature (T_H)) from one side (left vertical side) and cooled (low temperature (T_C)) from the adjacent side (top horizontal side) while the remaining walls are adiabatic. The average Nusselt numbers (Nu_{ave}) for various inclination and magnetic field orientation angles are listed in Table 2a. The numerical results obtained with the proposed scheme are in an excellent agreement with those using a Finite Volume Method (FVM) [4]. The comparison of the proposed scheme with the FVM showed that the maximum absolute error is 10^{-2}. As a second example we considered the natural convection in an enclosure that is filled with a water-Al_2O_3 nanofluid, influenced by a magnetic field. The enclosure is bounded by two isothermal vertical walls at temperatures T_h and T_c and by two horizontal adiabatic walls. The average and maximum absolute value for the stream function $|\Psi_{max}|$ with the solid volume fraction at different values of the Hartmann number (Ha) are listed in Table 3. The numerical results obtained by the present scheme are compared with those obtained using the Finite Volume Method (FVM) [30] and, it can be seen that they are in a very good agreement.(See Table 2b)

5. Numerical results

The heat performance of the micropolar-nanofluid filled enclosure is studied for a range of solid volume fractions $(0 \leqslant \varphi \leqslant 0.05)$, Rayleigh number $(10^4 \leqslant Ra \leqslant 10^6)$ to cover both buoyancy and magnetic field dominant flow regimes and, Hartmann number $(0 \leqslant Ha \leqslant 120)$. For all simulations, pure water is considered as the base fluid with $Pr = 6.2$ and the microrotation number was set to $K = 2$. The latter value has been chosen since, as depicted in [18], the numerical results are closer to the experimental findings. From the vorticity equation it can be seen that the magnitudes of Rayleigh (Ra) and Hartmann (Ha) numbers can regulate the buoyancy or the magnetic force dominant on the flow field inside the enclosure. In details, the buoyancy force is naturally more effective for higher Rayleigh numbers, where the Lorentz force reduces velocities and suppresses the convection currents. On the other hand, when $Ra/Ha^2 = O(1)$ both forces are equally effective. The buoyancy is dominant as long as $O(Ra/Ha^2) >> 1$ and the magnetic field is dominant when $O(Ra/Ha^2) << 1$. Finally, although the transient governing equations have been solved, we plot the steady state solutions of the governing equations.

5.1. The effects of the Rayleigh and Hartmann numbers

In this part of the study, an enclosure filled with Al_2O_3/water micropolar nanofluid is considered. In all the computations conducted, the solid volume fraction of the nanoparticles was constant and equal to $\varphi = 0.03$. Concerning the numerical computations, the Hartmann number was taken in the range of $0 \leqslant Ha \leqslant 120$, the inclination angle was $\gamma = 0^o$, while the angle of orientation of the magnetic field was taken also as $\xi = 0^o$ ($\boldsymbol{B} = B_0\boldsymbol{i}$). The Rayleigh number used was varied in the range of $10^4 \leqslant Ra \leqslant 10^6$ to cover the both buoyancy and magnetic field dominant flow regimes.

In Figs. 3 and 4 streamlines and temperature contours are shown, for two different values of the Hartmann number, namely

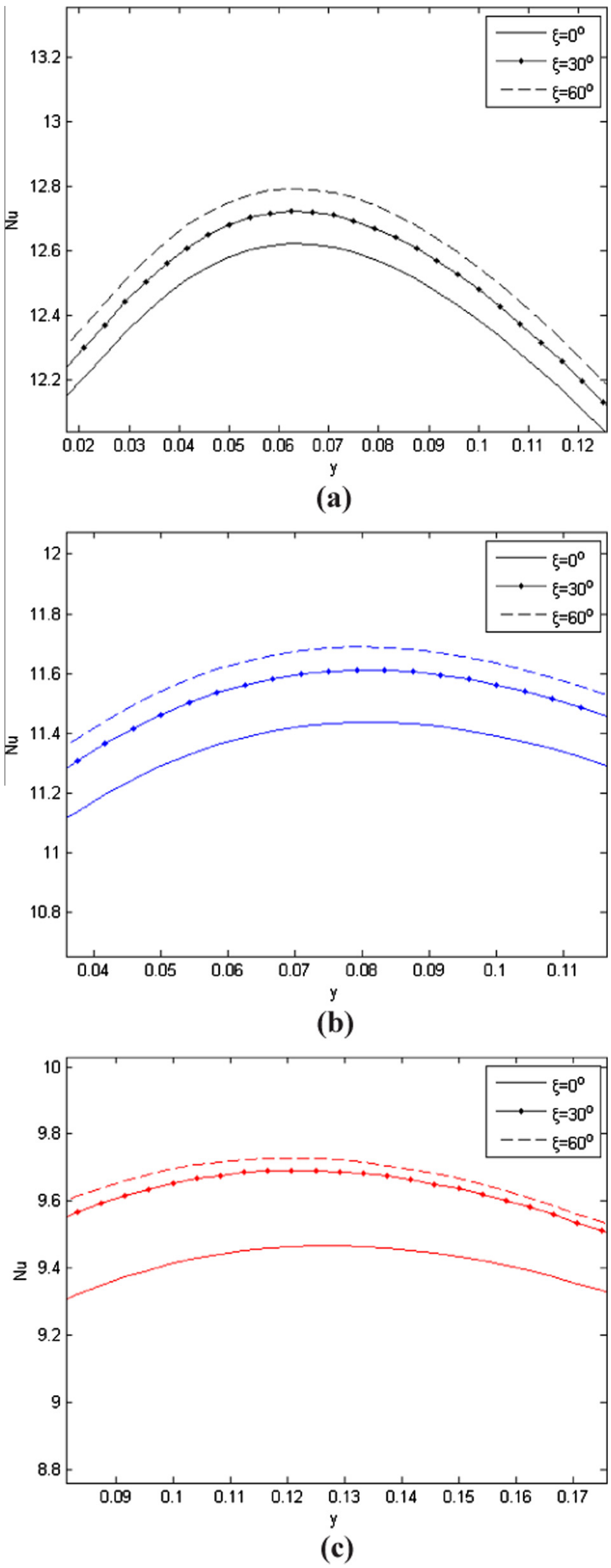

Fig. 11. Magnification of the local Nusselt number along the hot wall for different magnetic field orientation (ξ) angles for inclination angles **(a)** $\gamma = 0^o$ **(b)** $\gamma = 30^o$ and **(c)** $\gamma = 60^o$.

for $Ha = 60$ and $Ha = 120$, with the Rayleigh number ranging from $Ra = 10^4$ to $Ra = 10^6$. Since the enclosure is not inclined, the buoyancy force ascends the fluid particles heated near the hot wall, acts parallel to it and the streamlines form a single eddy with clockwise rotation. As far the isotherms, buoyancy force is more active lifting the warm fluid particles along the hot wall, the fluid then is forced to move horizontally along the adiabatic walls and, finally is descends when it reaches the cold vertical wall. As a result, the isotherms are closer to each other near the hot wall indicating higher surface heat flux and slightly bulged toward the cold wall due to the rapid transfer of heat by circulating fluid. The same pattern is evident in both Hartmann numbers and for all the Rayleigh numbers encountered. As it can be seen, as the *Ra* number increases the vortex that is formed in the middle of the cavity becomes more elongated to the *x*-direction. As the Hartmann number increases lower values of streamlines were observed. The flow patterns indicate lower values of the streamlines and weaker rotation due to the higher Hartmann number. The streamlines are bended in the region between $x = 0.2$ and $x = 0.8$ and as the Rayleigh number increases they tend orientate along with the *x*-axis direction, which is the magnetic field direction. This is also seen for $Ha = 60$ where the bending is more pronounced.

Fig. 5a shows the Local Nusselt number along the hot wall for various Rayleigh (*Ra*) and Hartmann (*Ha*) numbers. It can be seen that as the Rayleigh (*Ra*) number increases the local Nusselt number is shifted upwards. While, the increase of Hartmann (*Ha*) number shifts the local Nusselt number curves downwards.

In Fig. 5b the average Nusselt number was plotted against the Hartmann number, considering a micropolar nanofluid and a nanofluid without the microrotation. For a micropolar nanofluid it can be observed that for all the *Ra* numbers considered the average Nusselt number is smaller compared with that of a pure nanofluid model (this is thoroughly analyzed in [18]). It can be noticed that when the Rayleigh number is low ($Ra = 10^4$) the average Nusselt number (Nu_{ave}) is slightly different for the two models and slightly changed for everyone when the Hartmann number increases. As the Rayleigh number increases the Nu_{ave} is different for the two models and decreases as the *Ha* number increases.

5.2. The effects of solid volume fraction

In this part of the study, an enclosure filled with Al_2O_3/water micropolar nanofluid is considered. In all the computations conducted, the solid volume fraction of the nanoparticles was taken in the range of $0 \leqslant \varphi \leqslant 0.05$ along with the Hartmann number ranging from $Ha = 10$ to $Ha = 90$. The Rayleigh number was set to $Ra = 10^5$.

Fig. 6 shows the microrotation contours for with increasing solid volume fraction of the nanoparticles for different Hartmann numbers, namely $Ha = 30$ and $Ha = 60$. It can be seen that as the volume fraction of the nanoparticles increases the strength of the microrotation increases. In Fig. 7 the microrotation profiles are plotted along the centerlines of the cavity, at $y = 0.5$ and $x = 0.5$, respectively, for Hartmann numbers $Ha = 30$ and 60. Symmetric profiles are obtained, with the strength of the microrotation increasing as the volume fraction of the nanoparticles increases. This can be explained by the fact that the total amount of microrotation in the bulk is increased since the number of nanoparticles increases and consequently the total microrotation is elevated. Additionally, as it can be seen from Fig. 8, the average Nusselt number decreased as the volume fraction of nanoparticles increases. This is more evident as the Hartmann number is low. This can be explained by the fact that when the applied magnetic field (Hartmann number) is low the rotation of the particles remains without no intense mixing in the fluid. The exchange of heat energy with the solid wall is low and the Nusselt number is decreased. Notice that results show opposite behavior comparing with those of magnetite nanofluids under the influence of an external magnetic field [31]. That is, the increase of the magnetic field strength decreases the local heat transfer coefficient.

5.3. The effects of inclination angles

Microrotation contour lines in a square enclosure for $Ra = 10^6$, $Ha = 60$, $K = 2$, $\varphi = 0.03$ and various enclosure inclinations and magnetic field directions are shown in Fig. 9.

When the enclosure is tilted (30° and 60°) the buoyancy force forces fluid particles toward to and away from the hot wall is in the clockwise direction. Therefore, while the streamlines form a single eddy with clockwise rotation, the orientation and the strength of the eddy change. This can also be noticed when the magnetic field is not yet normal to the hot wall (30° and 60°), where the strength of the eddy increases as the inclination angle increases. The magnetic field applied normal to the hot wall is more effective reducing the convection and therefore the heat transfer for square and tall enclosures and the magnetic field applied normal to the cold wall is more effective reducing the convection for the enclosure. Fig. 10 shows the local Nusselt number along the hot wall for different inclination angles and orientation of the magnetic field. It can be seen that as the inclination angle (γ) increases the local Nusselt number is shifted downwards. In Fig. 11 a closer look of the local Nusselt number is shown and as the orientation angle (ξ) of the magnetic fields increases the local Nusselt number is up shifted.

6. Conclusions

The present study considers a numerical investigation of laminar natural-convection flow through an Al_2O_3/water micropolar nanofluid in the presence of a magnetic field in an inclined rectangular enclosure. The rotation of the nanoparticles was incorporated in the flow model. The mathematical theory that describes this particular flow regime is the micropolar flow theory that expresses apart from the conservation of linear momentum and angular momentum. Experimentally given forms of thermo-physical nanofluids's properties, as dynamic viscosity, thermal conductivity and electrical conductivity, are utilized. A meshless point collocation with velocity-correction method was utilized in order to numerically solve the governing equations. The study leads to the following conclusions:

- The flow characteristics and the convection heat transfer inside the tilted enclosure, depend strongly upon the strength and orientation of the magnetic field, the inclination of the enclosure, the microrotation number and the volume fraction of the nanoparticles used.
- Circulation and convection become stronger with increasing Rayleigh and microrotation numbers but they are significantly suppressed by the presence of a strong magnetic field.
- The local Nusselt number increases considerably with Rayleigh number since the circulation becomes stronger. The magnetic field significantly reduces the local Nusselt number by suppressing the convection currents.
- The local Nusselt number is shifted upwards as the Rayleigh (Ra) number increases. While, the local Nusselt number curves are shifted downwards as the Hartmann (Ha) number is increased.
- The presence of nanoparticles alters the thermal properties of the base fluid. For small values of nanoparticles's volume fraction ($\varphi < 0.02$) as the Hartmann number increases the average Nusselt is increased, while for ($\varphi > 0.02$) as the Hartmann number increases the average Nusselt is decreased.
- For a specific value of nanoparticles's volume fraction ($\varphi = 0.03$), as the Rayleigh (Ra) number increases the average Nusselt is increased, while as the Hartmann number increases and keeping (Ra) constant the average Nusselt is slightly decreased.
- For a micropolar nanofluid model it can be observed that for all the Rayleigh numbers considered the average Nusselt number was smaller compared with that of a pure nanofluid model.

Conflict of interest

None declared.

Appendix A

Solution procedure

Consider the governing equation of the unsteady problem

$$\frac{\partial q(\boldsymbol{x},t)}{\partial t} + \boldsymbol{L}q(x,t) = f(x,t), \quad \forall \boldsymbol{x} \in \boldsymbol{\Omega} \subset \mathbb{R}^3, \quad t > 0 \tag{A1}$$

$$\boldsymbol{B}q(\boldsymbol{x},t) = g(\boldsymbol{x},t), \quad \forall \boldsymbol{x} \in \partial\boldsymbol{\Omega} \subset \mathbb{R}^3, \quad \mathbf{t} > 0 \tag{A2}$$

where $\boldsymbol{L}$ is a differential operator and $\boldsymbol{B}$ is a boundary operator, which can be a Dirichlet, Neumann or a mixed operator. Using the notation $q^{(k+1)} = q(t^{(k+1)})$, where $t^{(k+1)} = t^{(k)} + \delta t$ and introducing θ-weighting $(0 \leqslant \theta \leqslant 1)$, we get

$$\frac{q^{(k+1)} - q^{(k)}}{\delta t} + \theta \boldsymbol{L} q^{(k+1)} + (1-\theta)\boldsymbol{L} q^{(k)} = h^{(k+1)} \tag{A3}$$

For the vorticity transport equation, the microrotation and the temperature equations under consideration the $\boldsymbol{L}$ operator is given by

$$L^{\Omega} = U\frac{\partial}{\partial X} + V\frac{\partial}{\partial Y} - \left(\frac{\mu_{nf}}{\mu_f} + K\right)\left(\frac{\rho_f}{\rho_{nf}}\right)\nabla^2 \tag{A4}$$

$$L^{N} = U\frac{\partial}{\partial X} + V\frac{\partial}{\partial X} - \left(\frac{\mu_{nf}}{\mu_f} + \frac{K}{2}\right)\left(\frac{\rho_f}{\rho_{nf}}\right)\nabla^2 + 2K\left(\frac{\rho_f}{\rho_{nf}}\right) \tag{A5}$$

$$L^{\theta} = U\frac{\partial}{\partial X} + V\frac{\partial}{\partial X} - \left(\frac{k_{nf}}{k_f}\right)\left(\frac{(\rho C_p)_f}{(\rho C_p)_{nf}}\right)\frac{1}{Pr}\nabla^2 \tag{A6}$$

and the right-hand side by

$$\begin{aligned} h^{\Omega} = & -K\left(\frac{\rho_f}{\rho_{nf}}\right)\nabla^2 N + \frac{Ra}{Pr}\left(\frac{(\rho\beta)_{nf}}{(\rho\beta)_f}\right)\left(\frac{\rho_f}{\rho_{nf}}\right)\left(\cos(\gamma)\frac{\partial\theta}{\partial X} - \sin(\gamma)\frac{\partial\theta}{\partial Y}\right) \\ & + \left(\frac{\sigma_{nf}}{\sigma_f}\right)\left(\frac{\rho_f}{\rho_{nf}}\right)Ha^2\left(\sin(\xi)\cos(\xi)\frac{\partial U}{\partial X} - \cos^2(\xi)\frac{\partial V}{\partial X}\right) \\ & + \left(\frac{\sigma_{nf}}{\sigma_f}\right)\left(\frac{\rho_f}{\rho_{nf}}\right)Ha^2\left(\sin^2(\xi)\frac{\partial U}{\partial Y} - \sin(\xi)\cos(\xi)\frac{\partial V}{\partial Y}\right) \end{aligned} \tag{A7}$$

$$h^{N} = K\left(\frac{\rho_f}{\rho_{nf}}\right)\Omega \tag{A8}$$

$$h^{\theta} = 0 \tag{A9}$$

For illustration purposes we will describe in details the linearization procedure used only for the vorticity. For now on we will use a notation $(r_{,s})$ for the derivatives defined as differentiation of the variable r with respect to s. The Eq. (A3) using Eq. (A4) can be written as

$$\begin{aligned} & \frac{\Omega^{(k+1)} - \Omega^{(k)}}{\delta t} + \vartheta\left((U\Omega_{,x})^{(k+1)} + (V\Omega_{,y})^{(k+1)} - \left(\frac{\mu_{nf}}{\mu_f} + K\right)\left(\frac{\rho_f}{\rho_{nf}}\right)\right. \\ & \left.\left(\Omega_{,xx}^{(k+1)} + \Omega_{,yy}^{(k+1)} +\right)\right) + (1-\vartheta)\left((U\Omega_{,x})^{(k)} + (V\Omega_{,y})^{(k)} - \left(\frac{\mu_{nf}}{\mu_f} + K\right)\right. \\ & \left.\left(\frac{\rho_f}{\rho_{nf}}\right)\left(\Omega_{,xx}^{(k)} + \Omega_{,yy}^{(k)} +\right)\right) = \left(h^{\Omega}\right)^{(k+1)} \end{aligned} \tag{A10}$$

Please cite this article in press as: G.C. Bourantas, V.C. Loukopoulos, MHD natural-convection flow in an inclined square enclosure filled with a micropolar-nanofluid, Int. J. Heat Mass Transfer (2014), http://dx.doi.org/10.1016/j.ijheatmasstransfer.2014.08.075

Following we linearize the non-linear terms of the Eq. (40) as

$$(U\Omega_{,i})^{(k+1)} \cong U^{(k)}\Omega_{,i}^{(k+1)} + U^{(k+1)}\Omega_{,i}^{(k)} - U^{(k)}\Omega_{,i}^{(k)} \tag{A11}$$

with $i = x,y$. Substituting Eq. (A11) in Eq. (A10), multiplying by δt and after collecting the $(k+1)$ and the (k) terms on the left and the right hand side, respectively, we get

$$\begin{aligned}&\Omega^{(k+1)} + \delta t\vartheta\left(U^{(k)}\Omega_{,x}^{(k+1)} + V^{(k)}\Omega_{,y}^{(k+1)} - \left(\frac{\mu_{nf}}{\mu_f} + K\right)\left(\frac{\rho_f}{\rho_{nf}}\right)\right.\\ &\left.\left(\Omega_{,xx}^{(k+1)} + \Omega_{,yy}^{(k+1)}\right)\right) = \Omega^{(k)} - \delta t\vartheta\left(\left(U^{(k+1)} - U^{(k)}\right)\Omega_{,x}^{(k)}\right.\\ &\left.+\left(V^{(k+1)} - V^{(k)}\right)\Omega_{,y}^{(k)}\right) - \delta t(1-\vartheta)\left(U^{(k)}\Omega_{,x}^{(k)} + V^{(k)}\Omega_{,y}^{(k)} - \left(\frac{\mu_{nf}}{\mu_f} + K\right)\right.\\ &\left.\left(\frac{\rho_f}{\rho_{nf}}\right)\left(\Omega_{,xx}^{(k)} + \Omega_{,yy}^{(k)}\right)\right) + \delta t(h^{\Omega})^{(k+1)}\end{aligned} \tag{A12}$$

Eq. (A12) can be written in matrix notation as

$$\mathbf{M}\Omega^{(k+1)} = (\mathbf{R} + \mathbf{Q})\Omega^{(k)} + \mathbf{F} \tag{A13}$$

where

$$\mathbf{M} = \begin{bmatrix} \mathbf{\Phi}^d + \delta t\vartheta^*(U^{(k)}\circ\mathbf{\Phi}_{,x}^d + V^{(k)}\circ\mathbf{\Phi}_{,y}^d - \left(\frac{\mu_{nf}}{\mu_f} + K\right)\left(\frac{\rho_f}{\rho_{nf}}\right) * (\mathbf{\Phi}_{,xx}^d + \mathbf{\Phi}_{,yy}^d)) \\ \mathbf{\Phi}^b \end{bmatrix} \tag{A14}$$

$$\mathbf{R} = \begin{bmatrix} -\delta t\vartheta^*((U^{(k+1)} - U^{(k)})\circ\mathbf{\Phi}_{,x}^d + (V^{(k+1)} - V^{(k)})\circ\mathbf{\Phi}_{,y}^d) \\ 0 \end{bmatrix} \tag{A15}$$

$$\mathbf{Q} = \begin{bmatrix} \Phi^d - \delta t(1-\vartheta) * \left(U^{(k)}\circ\Phi_{,x}^d + V^{(k)}\circ\Phi_{,y}^d - \left(\frac{\mu_{nf}}{\mu_f} + K\right)\left(\frac{\rho_f}{\rho_{nf}}\right) * \left(\Phi_{,xx}^d + \Phi_{,yy}^d\right)\right) \\ 0 \end{bmatrix} \tag{A16}$$

$$\mathbf{F} = \begin{bmatrix} \delta t(h^{\Omega})^{(k+1)} \\ \mathbf{g}^{(k+1)} \end{bmatrix} \tag{A17}$$

where matrices $\mathbf{\Phi}$, $\mathbf{\Phi}_{,s}$, $\mathbf{\Phi}_{,ss}$, with $s = x,y$, give the unknown field function approximation values and their spatial derivatives up to second order and $\mathbf{g}$ are the boundary conditions. These matrices can be written as $\mathbf{\Phi} = \begin{bmatrix} \mathbf{\Phi}^{N_d} \\ \mathbf{\Phi}^{N_b} \end{bmatrix} \in \mathbf{R}^{N\times N}$, corresponding to N_d interior nodes and N_b boundary nodes ($N = N_d + N_b$), with N being the total number of nodes. The symbol ($w^\circ D$) means that the i^{th} component of the vector w is multiplied to every element of the i^{th} row of the matrix $\boldsymbol{D}$.

References

[1] N. Rudraiah, R.M. Barron, M. Venkatachalappa, C.K. Subbaraya, Effect of a magnetic field on free convection in a rectangular enclosure, Int. J. Eng. Sci. 33 (1995) 1075–1084.

[2] S. Alchaar, P. Vasseur, E. Bilgen, Natural convection heat transfer in a rectangular enclosure with a transverse magnetic field, J. Heat Trans. 117 (1995) 668–673.

[3] J.P. Garandet, T. Alboussiere, R. Moreau, Buoyancy driven convection in a rectangular enclosure with a transverse magnetic field, Int. J. Heat Mass Transfer 35 (1992) 741–748.

[4] M.C. Ece, E. Buyuk, Natural-convection flow under a magnetic field in an inclined rectangular enclosure heated and cooled on adjacent walls, Fluid Dyn. Res. 38 (2006) 564–590.

[5] S. Sivasankaran, C.J. Ho, Effect of temperature dependent properties on MHD convection of water near its density maximum in a square cavity, Int. J. Therm. Sci. 47 (2008) 1184–1194.

[6] P. Kandaswamy, S.M. Sundari, N. Nithyadevi, Magnetoconvection in an enclosure with partially active vertical walls, Int. J. Heat Mass Transfer 51 (2008) 1946–1954.

[7] M. Pirmohammadi, M. Ghassemi, Effect of magnetic field on convection heat transfer inside a tilted square enclosure, Int. Commun. Heat Mass Transfer 36 (2009) 776–780.

[8] S.U.S. Choi, J.A. Eastman, Enhancing thermal conductivity of fluids with nanoparticles, in: D.A. Siginer, H.P. Wang (Eds.), Development and Application of Non-Newtonian Flows, American Society of Mechanical Engineers, New York, 1995, pp. 99–105.

[9] K. Khanafer, K. Vafai, M. Lightstone, Buoyancy-driven heat transfer enhancement in a two-dimensional enclosure utilizing nanofluids, Int. J. Heat Mass Transfer 46 (2003) 3639–3653.

[10] E. Abu-Nada, Z. Masoud, A. Hijazi, Natural convection heat transfer enhancement in horizontal concentric annuli using nanofluids, Int. Commun. Heat Mass Transfer 35 (2008) 657–665.

[11] H.F. Oztop, E. Abu-Nada, Numerically study of natural convection in partially heated rectangular enclosures filled with nanofluids, Int. J. Heat Fluid Flow 29 (2008) 1326–1336.

[12] S.M. Aminossadati, B. Ghasemi, Enhanced natural convection in an isosceles triangular enclosure filled with a nanofluid, Comput. Math. Appl. 61 (2011) 1739–1753.

[13] A.G. Nnanna, Experimental model of temperature-driven nanofluid, J. Heat Transfer 129 (2006) 697–704.

[14] H.F. Oztop, E. Abu-Nada, Numerical study of natural convection in partially heated rectangular enclosures filled with nanofluids, Int. J. Heat Fluid Flow 29 (2008) 1326–1336.

[15] S.M. Aminossadati, B. Ghasemi, Natural convection cooling of a localised heat source at the bottom of a nanofluid-filled enclosure, Eur. J. Mech.B. Fluids 28 (2009) 630–640.

[16] A.K. Santra, S. Sen, N. Chakraborty, Study of heat transfer characteristics of copper-water nanofluid in a differentially heated square cavity with different viscosity models, J. Enhanced Heat Transfer 15 (2008) 273–287.

[17] A.C. Eringen, Simple microfluidics, Int. J. Eng. Sci. 2 (2) (1964) 205–217.

[18] G.C. Bourantas, V.C. Loukopoulos, Modeling the natural convective flow of micropolar nanofluids, Int. J. Heat Mass Transfer 68 (2014) 35–41.

[19] M. Zadravec, M. Hribersek, L. Skerget, Natural convection of micropolar fluid in an enclosure with boundary element method, Engng. Anal. Boundary Elem. 33 (2009) 485–492.

[20] J.A. Shercliff, A Textbook on Magnetohydrodynamics, Pergamon Press, Oxford, 1965.

[21] G. Ahmadi, Self-similar solution of incompressible micropolar boundary layer flow over a semi-infinite flat plate, Int. J. Eng. Sci. 14 (1976) 639–646.

[22] D.A.S. Rees, I. Pop, Free convection boundary-layer flow of a micropolar fluid from a vertical flat plate, IMA J. Appl. Math. 61 (1998) 179–197.

[23] B.C. Pak, Y.I. Cho, Hydrodynamic and heat transfer study of dispersed fluid with submicron metallic oxide particles, Exp. Heat Transfer 11 (1998) 151–170.

[24] K.F.V. Wong, T. Kurma, Transport properties of alumina nanofluids, Nanotechnology 19 (2008) 345702.

[25] P. Lancaster, K. Salkauskas, Surfaces generated by moving least squares method, Math. Comput. 37 (155) (1981) 141–158.

[26] G.R. Liu, Mesh Free Methods, CRC Press, Moving beyond the Finite Element Method, 2002.

[27] S.N. Atluri, S.P. Shen, The Meshless Local Petrov–Galerkin (MLPG) Method, 440 pages, Tech Science Press, Encino USA, 2002.

[28] G.C. Bourantas, E.D. Skouras, V.C. Loukopoulos, G.C. Nikiforidis, Meshfree point collocation schemes for 2D steady state incompressible Navier–Stokes equations in velocity-vorticity for higher Reynolds number, CMES- Comput. Model. Eng. Sci. 59 (2010) 31–63.

[29] G.C. Bourantas, V.N. Burganos, An implicit meshless scheme for the solution of transient non-linear Poisson type equations, Eng. Anal. Boundary Elem. 37 (2013) 1117–1126.

[30] B. Ghasemi, S.M. Aminossadati, A. Raisi, Magnetic field effect on natural convection in a nanofluid-filled square enclosure, Int. J. Therm. 50 (2011) 1748–1756.

[31] R. Azizian, E. Doroodchi, T. McKrell, J. Buongiorno, L.W. Hu, B. Moghtaderi, Effect of magnetic field on laminar convective heat transfer of magnetite nanofluids, Int. J. Heat Mass Transfer 68 (2014) 94–109.